

Autonomous Robotic System for High-Efficiency Non-Destructive Bridge Deck Inspection and Evaluation

Hung M. La, Ronny S. Lim, Basily Basily, Nenad Gucunski, Jingang Yi, Ali Maher, Francisco A. Romero, and Hooman Parvardeh

Abstract—Bridges are one of the critical civil infrastructure for safety of traveling public. The conditions of bridges deteriorate with time as a result of material aging, excessive loading, and inadequate maintenance, etc. In this paper, the development of an autonomous robotic system is presented for highly-efficient bridge deck inspection and evaluation. An autonomous mobile robot is used as a platform to carry various non-destructive evaluation (NDE) sensing systems for simultaneous and fast data collection. Besides the NDE sensors, the robot is also equipped with various onboard navigation sensors. A sensing integration scheme is presented for high-accuracy robot localization and navigation. The effectiveness of the autonomous robotic NDE system is demonstrated through extensive experiments and field deployments.

I. INTRODUCTION

Bridges are one of the infrastructure components critical for the safety of traveling public and sustainability of the economic activity. Their conditions deteriorate with time as a result of material aging, excessive use and overloading, environmental conditions and inadequate maintenance, etc [1]. Effective health monitoring, maintenance, repair and replacement of the deteriorating bridge components are necessary to ensure the transportation safety. Non-destructive evaluation (NDE) is one of the effective ways to reliably identify and predict early-stage bridge deterioration to enable proactive interventions for repair and rehabilitation. There are a number of NDE technologies that are currently being used in bridge evaluation, including impact echo, ground penetrating radar (GPR), electrical resistivity, visual inspection, etc. [2], [3]. Fig. 1 shows a typical application of NDE technologies in bridge deck inspection. When NDE is conducted on bridge decks, a section of the bridge is closed for traffic causing inconvenient traffic slow-down. The delivery of the current NDE technologies cannot meet the increasing demands for highly-efficient, cost-effective

This work was supported in part by the US National Institute of Standards and Technology (NIST) Technology Innovation Program (TIP) under award 70NANB10H014.

H. M. La, R. S. Lim, F. A. Romero, and H. Parvardeh are with the Center for Advanced Infrastructure and Transportation (CAIT), Rutgers University, Piscataway, NJ 08854 USA (email: hung.la11@rutgers.edu, ronny.lim@rutgers.edu, faromero@rci.rutgers.edu, hoomanp@rci.rutgers.edu).

B. Basily is with the Department of Industrial and Systems Engineering, Rutgers University, Piscataway, NJ 08854 USA (email: basily@rci.rutgers.edu).

N. Gucunski and A. Maher are with the Department of Civil and Environmental Engineering, Rutgers University, Piscataway, NJ 08854 USA (email: gucunski@rci.rutgers.edu, mmaher@rci.rutgers.edu).

J. Yi is with the Department of Mechanical and Aerospace Engineering, Rutgers University, Piscataway, NJ 08854 USA (email: jgyi@rutgers.edu).

inspection due to intensive labor work and negative impact on the traffic flow.



Fig. 1. The state-of-the-art of the NDE technology for bridge deck inspection and evaluation.

The goal of this paper is to present the development and demonstration of a new autonomous robotic system for high-efficiency bridge deck inspection and evaluation. Robotics and automation technologies have gained increasingly applications in civil infrastructure in the past two decades. For example, mobile robot- or vehicle-based inspection systems were developed for cracks detection and maintenance for highways [4], [5]. The mobile manipulator systems were used to extend the capability of human inspectors for bridge crack inspection [6] and rehabilitation [7], [8]. Similar systems were developed for vision-based automatic crack detection and mapping for bridge decks [9], [10]. Despite all of the above-mentioned developments, to the best of the authors' knowledge, no autonomous robotic system is developed to deploy and integrate multiple NDE technologies for high-efficiency and high-accuracy bridge deck condition assessment.

One of the challenging tasks to develop an autonomous robot for bridge deck inspection is a robust, reliable localization and navigation system. Since the robot movement needs to cover the narrow deck surface, it is required that the localization and navigation accuracy must be within a range of a few centimeters. Although high-accuracy global positioning system (GPS) with real-time kinematic (RTK) correction can reach the requirement, GPS signals are not always reliable and robust, especially on bridges with partial coverage, steel cables, truss elements or other support structures. Similar to the approaches in [11], dual RTK GPS antennas are used on the mobile robot platform. The GPS measurements are

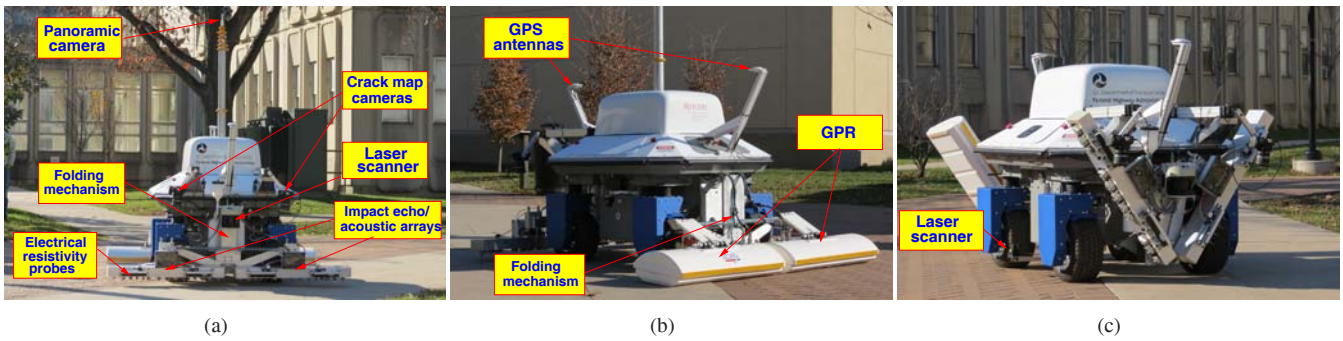


Fig. 2. The Rutgers robotic bridge deck diagnosis system. (a) The front view of the system while the NDE sensors are at working position. (b) The rear view of the robotic system. (c) The side view of the robotic system when the NDE sensors are at idle position.

integrated with attitude information from the inertial measurement unit (IMU) to enhance the localization accuracy. Moreover, the GPS/IMU measurements are also fused with the wheel odometry through an extended Kalman filter (EKF) design [12], [13] for high-accuracy localization that meets the inspection requirements even in GPS-denied environments.

The main contribution of the presented work lies in the new autonomous robotic system for highly-efficient NDE of bridge decks. The robotic system is the first of this kind that integrates the state-of-the-art robotics and NDE technologies. The performance of the robotic system enables fast data collection and highly-accurate bridge deck inspection and evaluation as well as the cost and time reduction.

The rest of this paper is organized as follows. In Section II, descriptions of the robotic NDE system are presented. In Section III, the robot localization and navigation system is discussed. The experimental results are presented in Section IV before we conclude the paper in Section V.

II. ROBOTIC NDE SYSTEM

A. System Overview

The robotic system with the integrated NDE technologies is shown in Fig. 2. The mobile platform is a Seekur robot from Adept Mobile Robot Inc. The Seekur robot is an electrical all-wheel driving and steering platform. Such a mobile robot was chosen primarily because of the required high-agility motions, such as zero-turning-radius maneuver on narrow bridge decks. The control hierarchy for the mobile robot consists of two layers: the lower-level real-time robot controllers are provided by the vendor and the upper level control is supplied by users. The upper-level controller provides the desired linear velocity and the yaw angle values for the robot, while the lower-level controller takes these commanded values and drives the motors for robot motion.

The mobile robot has been modified and equipped with various sensors, actuators, and computing devices. Two sets of sensor suites are equipped on the robot: navigation sensors and NDE sensors. The navigation sensors include two RTK GPS units (from Novatel Inc.), one front- and two side-mounted laser scanners (from Sick AG and Hokuyo Automation Co., respectively), and one IMU sensor (from Microstrain Inc.) These laser scanners are mainly used for robot obstacle avoidance and safe operation. The onboard NDE

sensors include two GPR units, two seismic/acoustic array sensors, four electrical resistivity probes, two high-resolution cameras and a 360-degree panoramic camera.

Three industrial standard embedded computers (from Versalogic Inc.) are installed inside the robot. One computer runs Robotic Operating System (ROS) for the robot navigation and motion planning tasks. The other two computers use Windows operating system for integrating the NDE sensors and data collection. High-speed Ethernet connections are used among these computers and each computer can also be reached individually through high-speed wireless communication by remote computers. The remote visualization and data analysis computers are located inside a full-size cargo van that is also used for transporting the robotic system.

Some NDE sensors including seismic/acoustic sensors and electrical resistivity probes need to be in contact with the deck surface for measurement. Therefore, a set of actuators were built to move these NDE sensors up from and down to the deck surface. Typically, the robot moves and stops at a certain distance (e.g., 0.6 m) for NDE data collection. After the robot stops, the NDE sensor probes are coupled to the deck surface, and when the data collection is finished, the NDE probes are lifted up and the robot is ready to move to the next planned inspection point. The motion coordination between the NDE sensors and the robot navigation is built through the control algorithms.

B. Robotic NDE Systems

1) *NDE technologies for bridge deck inspection*: The NDE technologies are used in a complementary manner to provide comprehensive inspection information [2].

Ground penetrating radar (GPR): GPR is a geophysical method that uses radar pulses to image the subsurface. The GPR system uses high-frequency electromagnetic waves and transmits them into the ground. When the waves encounter objects or materials of different dielectric properties, such as rebars, the waves are reflected and detected by a receiving antenna. The GPR usually assesses the condition of concrete bridge decks based on the attenuation of electromagnetic waves on the top rebar level [14]. The developed robotic system utilizes Hi-Bright ground-coupled GPR arrays manufactured by IDS Italy.

Impact echo: The impact echo method is used for detection of discontinuities and for element thickness evaluation of

concrete and masonry elements. It is a seismic resonant method and is primarily used to detect and characterize delamination (horizontal cracking) in bridge decks with respect to depth, spread and severity. It can be also used to detect debonding of overlays on bridge decks. The robotic system integrates more than a dozen impact echo sensors.

Electrical resistivity: Electrical resistivity sensor measures concrete’s electrical resistivity, which is a reflection of the corrosive environment of the bridge deck. The presence of water, chlorides, salts or other contaminants reduces concrete’s resistivity, and facilitates corrosive processes in bridge decks. By measuring the electrical resistivity, the corrosion rate of reinforcing rebars can be estimated.

Visual detection of surface cracks: Developing a reliable and robust vision-based crack detection and mapping system is a challenging task due to the variations of outdoor environment, such as illumination conditions etc. The robotic system uses two cameras for crack detection and one panoramic camera with a 360-degree field of view to capture the surveyed area. The panoramic camera is mounted on a computer-controlled, extendable mast.

2) *Mechatronic design for robotic NDE sensor integration:* The use of a large number of NDE sensors enables scanning of 1.8 m wide area of a bridge deck during a single robot pass. Distribution and placement of the NDE sensors on the robot should take serious consideration due to the limited onboard battery capacity and payload (less than 150 kg). The footprint of the robotic system also needs to be kept compact for transportation and storage.

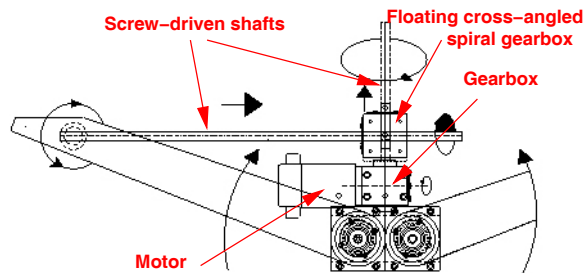


Fig. 3. Folding mechanism to extend and retreat the GPS antennas, impact echo/acoustic arrays and electrical resistivity probes.

To meet the design requirements, a mechanical folding mechanism was developed for the robotic NDE sensor integration. Fig. 3 illustrates the folding mechanism to extend and retreat the GPR arrays, seismic/acoustic arrays and electrical resistivity sensor suite to keep a compact robotic design. The folding mechanisms are installed on the front (for seismic/acoustic arrays and electrical resistivity sensors) and the rear (for the GPR antenna arrays) of the robot; see Fig. 2(a) and 2(b), respectively. Two swing arms lift the sensor units into a folded position through a screw-driven angled spiral gear box, as shown in Fig. 3. The floating gearbox is driven by a vertical screwed shaft powered by a high torque geared motor. Figs. 4(a) and 4(b) show the examples of folding and unfolding the seismic/acoustic arrays and the electrical resistivity sensors.

A pneumatically expanded telescopic mast is used to lift the panoramic camera up to a height of 4.5 m above the ground; see Fig. 4(d). The mast five telescopic segments provide a compact collapsed height that falls in line with robot platform as shown in Fig. 2. The deployment system for surface cracks inspection cameras consists of two non-rotating piston rod pneumatic cylinders; see Fig. 4(c). The entire deployment systems are controlled by the robot main computer, or manually through an override switch.

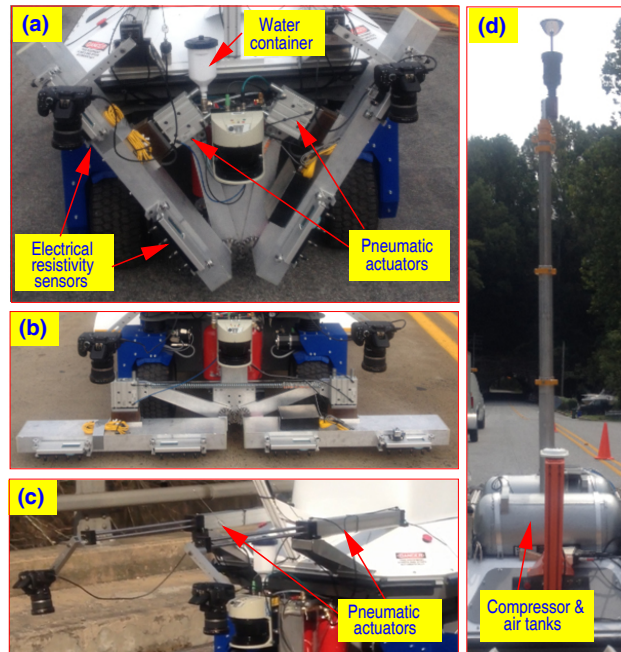


Fig. 4. Snapshots of mechatronic design for the NDE sensor/robot integration. (a) Folding position for the NDE sensors. (b) Unfolding and working position for the NDE sensors. (c) Extended position for the crack detection and mapping cameras. (d) Extended position of telescopic mast for the survey panoramic camera.

III. ROBOT NAVIGATION AND MOTION CONTROL

A. EKF-Based Robot Localization

To design a reliable, robust localization scheme, the GPS data are fused with the IMU and the wheel encoder measurements. An extended Kalman filter design is used to fuse these measurements. An inertial frame $\mathcal{I} : XYZ$ is defined on the bridge deck with the X -axis along the traffic flow direction and the Z -axis vertically upwards as shown in Fig. 5. The IMU is mounted around the center of the robot and the Euler angles $\Phi = [\phi_r \ \varphi_r \ \theta_r]^T$ are used to define the robot’s 3D attitude, where ϕ_r is the roll angle, φ_r pitch angle and θ_r yaw angle, as shown in Fig. 5(a). The two-dimensional position vector of the robot center in \mathcal{I} is denoted as $\mathbf{q}_r = [x_r \ y_r]^T$. Also, the yaw rate of the robot is denoted as ω_θ .

For simplicity, a precise kinematic model for omnidirectional robots (e.g., [15]) is not considered and instead we use the unicycle kinematic model for the robot motion,

$$\begin{cases} \dot{x}_r = v_r \cos \theta_r = v_r c_{\theta_r} \\ \dot{y}_r = v_r \sin \theta_r = v_r s_{\theta_r} \end{cases} \quad (1)$$

where v_r is the magnitude of the linear velocity \mathbf{v}_r and notations $c_{\theta_r} := \cos \theta_r$ and $s_{\theta_r} := \sin \theta_r$ are used for angle

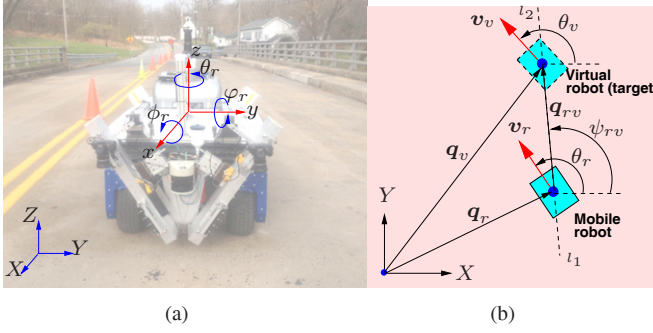


Fig. 5. (a) Robot attitude coordinates. (b) Schematic of virtual robot tracking design.

θ_r and other angles in the rest of the paper. To estimate the robot's attitude, the IMU measurements are used. The angular rate measurements of the IMU are denoted as $\Omega = [\omega_x \ \omega_y \ \omega_z]^T$ in the IMU frame. The kinematic equations for the IMU motion are written as follows [13].

$$\dot{\phi}_r = \omega_x + \omega_y s_{\phi_r} \tan \varphi_r + \omega_z c_{\phi_r} \tan \varphi_r, \quad (2a)$$

$$\dot{\varphi}_r = \omega_y c_{\phi_r} + \omega_z s_{\phi_r}, \quad (2b)$$

$$\dot{\theta}_r = \frac{s_{\phi_r} \omega_y}{c_{\varphi_r}} + \frac{c_{\phi_r} \omega_z}{c_{\varphi_r}}. \quad (2c)$$

The discrete-time representation of the state variables is

$$\mathbf{X}(k) = [x_r(k) \ y_r(k) \ v_r(k) \ \omega_\theta(k) \ \phi_r(k) \ \varphi_r(k) \ \theta_r(k)]^T$$

at the k th step. The kinematic motions given in (1) and (2) are linearized and the dynamic model is obtained as

$$\mathbf{X}(k+1) = \mathbf{A}\mathbf{X}(k) + \mathbf{B}\mathbf{u}(k) + \mathbf{w}(k), \quad (3)$$

where matrices \mathbf{A} and \mathbf{B} are given as

$$\mathbf{A} = \begin{bmatrix} 1 & 0 & T c_{\theta_r} & 0 & 0 & -T v_r s_{\theta_r} & 0 \\ 0 & 1 & T s_{\theta_r} & 0 & 0 & T v_r c_{\theta_r} & 0 \\ 0 & 0 & 1 & 0 & 0 & 0 & 0 \\ 0 & 0 & 0 & 1 & 0 & 0 & 0 \\ 0 & 0 & 0 & 0 & 1 + T \dot{\varphi}_r \tan \varphi_r & \frac{T \dot{\theta}_r}{c_{\varphi_r}} & 0 \\ 0 & 0 & 0 & 0 & -T \dot{\theta}_r c_{\varphi_r} & 1 & 0 \\ 0 & 0 & 0 & 0 & \frac{T \dot{\varphi}_r}{c_{\varphi_r}} & T \dot{\theta}_r \tan \varphi_r & 1 \end{bmatrix}$$

$$\mathbf{B} = \begin{bmatrix} \frac{T^2}{2} & 0 & 0 & 0 & 0 & 0 & 0 \\ 0 & \frac{T^2}{2} & 0 & 0 & 0 & 0 & 0 \end{bmatrix}^T,$$

$T = 1$ ms is the sampling time, $\mathbf{u}(k) = [a_x(k) \ a_y(k)]^T$ is the acceleration of the robot motion along the X and Y directions, $\mathbf{w}(k) \sim \mathcal{N}(\mathbf{0}, \mathbf{Q}(k))$ is the Gaussian process noise with covariance $\mathbf{Q}(k) = \text{diag}\{\sigma_x^2(k) \ \sigma_y^2(k) \ \sigma_{v_r}^2(k) \ \sigma_{\omega_\theta}^2(k) \ \sigma_{\phi_r}^2(k) \ \sigma_{\varphi_r}^2(k) \ \sigma_{\theta_r}^2(k)\}$. Comparing with (1), model (3) includes the robot acceleration $\mathbf{u}(k)$ to enhance the accuracy.

The measurement model of the system is

$$\mathbf{Y}(k) = \mathbf{H}(k)\mathbf{X}(k) + \mathbf{v}(k), \quad (5)$$

where $\mathbf{H}(k) = [\mathbf{I}_4 \ \mathbf{0}_{4 \times 3}]$, \mathbf{I}_n is an $n \times n$ identify matrix, and observation noises $\mathbf{v}(k)$ are assumed to be zero mean

Gaussian white signals with covariance matrix $\mathbf{R}(k)$, namely, $\mathbf{v}(k) \sim \mathcal{N}(\mathbf{0}, \mathbf{R}(k))$. The measurements are obtained as follows: positioning information (x_r, y_r) are obtained from the RTK GPS, the robot's linear velocity v_r and the yaw angular velocity ω_θ are obtained by the lower-level robot controller. The covariance matrix $\mathbf{R}(k)$ is tuned in the EKF design using the specification data provided by the GPS, the IMU and the robot vendors. Using the state dynamic model (3) and output (5), an EKF was designed to estimate the robot positioning information (x_r, y_r) and attitude heading θ_r .

B. Motion Planning and Control

The goal of the motion planning and control is to generate the desired trajectory for the robot and then to control the robot to follow the trajectory accurately. The inspected bridge is assumed to be straight and the bridge deck area is assumed to be a rectangular shape. The robot motion planning is indeed a coverage planning problem [16]. A boustrophedon decomposition, also the so-called "ox plowing motion" or trapezoidal decomposition in robotics research, is used. Fig. 6 illustrates the robot motion on the bridge. To cover the desired deck area, three GPS waypoints are first obtained at the rectangle corners such as points A , B , and C . Using the GPS waypoints of these three corners, the zigzag shape motion trajectories (with interpolated waypoints) for the robot are computed by the trapezoidal decomposition algorithm, as the arrows indicated in the figure.



Fig. 6. Schematic of motion planning of the inspection robot on a bridge (the picture shown here is the top view of the Pohatcong Creek Bridge near the township of Bloomsbury, Warren county, New Jersey, USA.)

An artificial potential field approach is used to design the robot motion control to follow the trajectory. It is considered that a virtual robot is moving along the desired trajectory and the virtual robot generates an attractive force to the inspection robot to follow. Fig. 5(b) illustrates the concept of the virtual robot following design. The robots' velocity directions are assumed to be aligned with their heading directions for simplicity.

The velocity vector of the robot center is denoted as $\mathbf{v}_r \in \mathbb{R}^2$, and the position vector, the velocity vector, and the yaw angle of the virtual robot in frame \mathcal{I} are denoted as $\mathbf{q}_v = [x_v \ y_v]^T \in \mathbb{R}^2$, $\mathbf{v}_v = \dot{\mathbf{q}}_v$, and θ_v , respectively. The relative position vector and angle from the mobile robot to the virtual robot are defined as $\mathbf{q}_{rv} = [x_{rv} \ y_{rv}]^T$ and φ_{rv} , respectively; see Fig. 5(b). The value of \mathbf{q}_{rv} is calculated as $x_{rv} = x_v - x_r$ and $y_{rv} = y_v - y_r$. Similarly, the relative velocity $\mathbf{v}_{rv} = [\dot{x}_{rv} \ \dot{y}_{rv}]^T$ are computed as $\dot{x}_{rv} = \|\mathbf{v}_v\|_2 c_{\theta_v} - \|\mathbf{v}_r\|_2 c_{\theta_r}$ and $\dot{y}_{rv} = \|\mathbf{v}_v\|_2 s_{\theta_v} - \|\mathbf{v}_r\|_2 s_{\theta_r}$.

The goal of the tracking controller is to regulate $\|\mathbf{q}_{rv}\|$ to zero as fast as possible. To achieve such a design,

the potential field approach [17] is used and an attractive potential function is defined as

$$U_a = \frac{1}{2}\alpha\|\mathbf{q}_{rv}\|^2 = \frac{1}{2}\alpha\mathbf{q}_{rv}^T\mathbf{q}_{rv},$$

where $\alpha > 0$ is a constant. To track the virtual robot with velocity \mathbf{v}_v , the robot controller is designed as

$$\mathbf{v}_r^d = \mathbf{v}_v + \nabla_{\mathbf{q}_{rv}} U_a = \mathbf{v}_v + \alpha\mathbf{q}_{rv}, \quad (6)$$

where $\nabla_{\mathbf{x}} U$ represents the gradient calculation of scalar U along vector \mathbf{x} . To track the virtual robot, the virtual robot's velocity must be within the forward direction relative to the actual robot, i.e., $|\theta_v - \varphi_{rv}| \leq \frac{\pi}{2}$; see Fig. 5(b). Thus, $c_{\theta_v - \varphi_{rv}} \geq 0$ and it can be shown that $\|\mathbf{v}_r^d\| \geq \|\mathbf{v}_v\|$.

It is also desirable to have the equal projected velocities of the virtual and actual robots along the direction perpendicular to line $l_1 l_2$ connecting their centers as shown in Fig. 5(b). Therefore, the relationship $\|\mathbf{v}_r\| s_{\theta_r - \varphi_{rv}} = \|\mathbf{v}_v\| s_{\theta_v - \varphi_{rv}}$ is obtained. From this relationship, the yaw angle controller for the mobile robot is obtained as

$$\theta_r^d = \varphi_{rv} + \sin^{-1} \left(\frac{\|\mathbf{v}_v\| s_{\theta_v - \varphi_{rv}}}{\|\mathbf{v}_r\|} \right). \quad (7)$$

When the value of $\|\mathbf{v}_r\|$ is near zero, a threshold value $\|\mathbf{v}_r\| = v_{r \min}$ is used for the calculation given in (7). The virtual robot's velocity profile \mathbf{v}_v is determined and generated by the inspection need. For example, in the filed deployment, the robot stops at each 0.6 m to take one NDE sensor measurement, especially for the impact echo and electrical resistivity sensors. It is also noted that the singularity issue discussed in [15] is avoided by the implementation restriction in the lower-level robot controllers.

IV. EXPERIMENTS AND FIELD DEPLOYMENT

A. Navigation Experiments

The robot navigation system was extensively tested on Rutgers Busch campus before it was deployed in the field. Fig. 7 illustrates one example of the comparison results of the navigation systems based on the EKF design discussed in Section III-A. It is clearly shown in the figure that the EKF-based navigation system over-performs the localization results based on the wheel odometry. It is noticed that when the robot is running near buildings and trees, the GPS data are not reliable. The top two sub-figures in Fig. 7 illustrate the comparison results of the EKF-based localization with those given by only GPS signal when there are trees or buildings nearby along the trajectory. It is clearly seen the noisy and distorted trajectories given by the GPS units. With the EKF-based sensor fusion, much more accurate localization information is achieved.

B. Field Deployment

The robotic NDE sensor arrays and probes were tested and their performance were validated on an actual bridge during summer and fall of 2012. The Pohatcong Creek Bridge near the township of Bloomsbury, Warren County, New Jersey, USA, was chosen for the field deployment site. The bridge

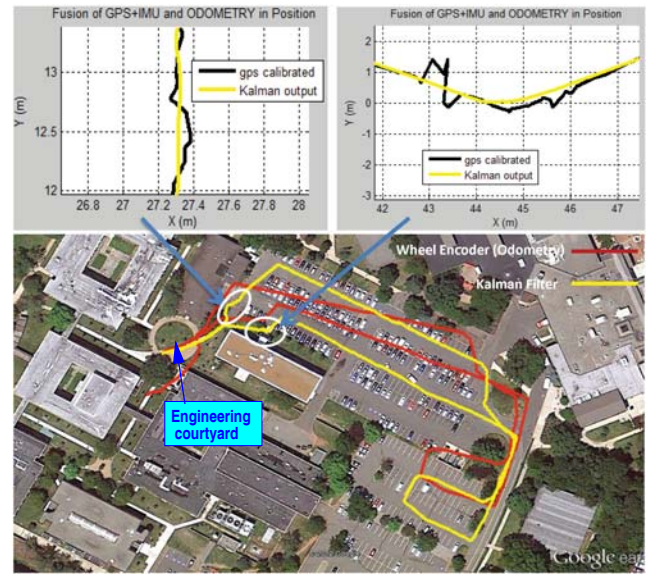


Fig. 7. Comparison of the navigation results by the EKF-based GPS/IMU/odometry fusion and the GPS and odometry-based localization on Rutgers Busch campus.

was built in 1970, and it has a bare concrete deck in a fair condition. The size of the Pohatcong Creek Bridge is about 160 feet (49 m) long and about 40 feet (12 m) wide. The top view of the bridge deck from Google Earth and the path during a robot maneuvering test are shown in Fig. 6. Three robotic scans were planned, as shown in the figure.

The testing results for the robot localization and navigation control are shown in Fig. 8. The virtual robot-based motion control design generated satisfactory trajectory-following results. For most of the time of the test run, the tracking errors were within 5-15 cm among the three scans of the bridge deck. The high-accuracy navigation enabled simultaneously deploying the NDE sensors and collecting data.

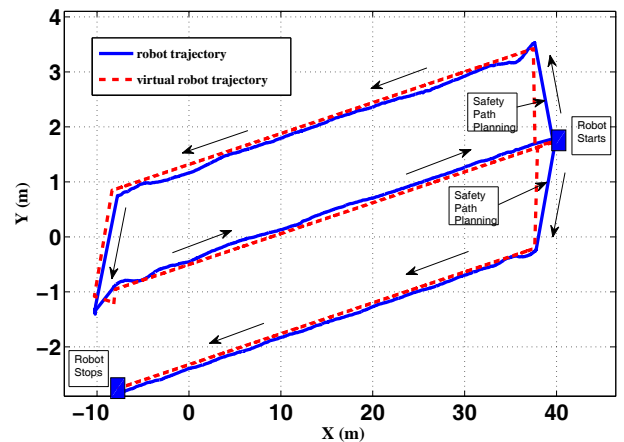


Fig. 8. Localization and navigation results on the Pohatcong Creek Bridge.

The NDE evaluation was conducted on various locations of the bridge deck surface to minimize local traffic interruptions. The NDE survey results for the bridge are shown in Fig. 9. The GPR condition and the electrical resistivity

maps in Figs. 9(a) and 9(c) show the survey results for the entire bridge deck while the impact echo condition map in Fig. 9(b) is only for a half bridge deck surface due to a slower data collection process than the other technologies. The numbers shown in these maps are calculated by using the NDE sensing data [2]. The plotting colors are based on these calculated numbers to indicate the different deterioration severity levels with respect to delamination, corrosion rate, and the overall condition. The benefits of having the condition maps from multiple complementary NDE sensors are obvious. For example, the GPR condition map in Fig. 9(a) indicates a large cluster of probable severe deterioration around locations at longitudinal/lateral positions (45, 10) ft and (90, 10) ft. The same locations are shown in Fig. 9(c) as zones of highly corrosive environment, and thus probable high corrosion rate. These correlations confirm that the primary cause of deterioration and delamination is the highly corrosive conditions at these locations.

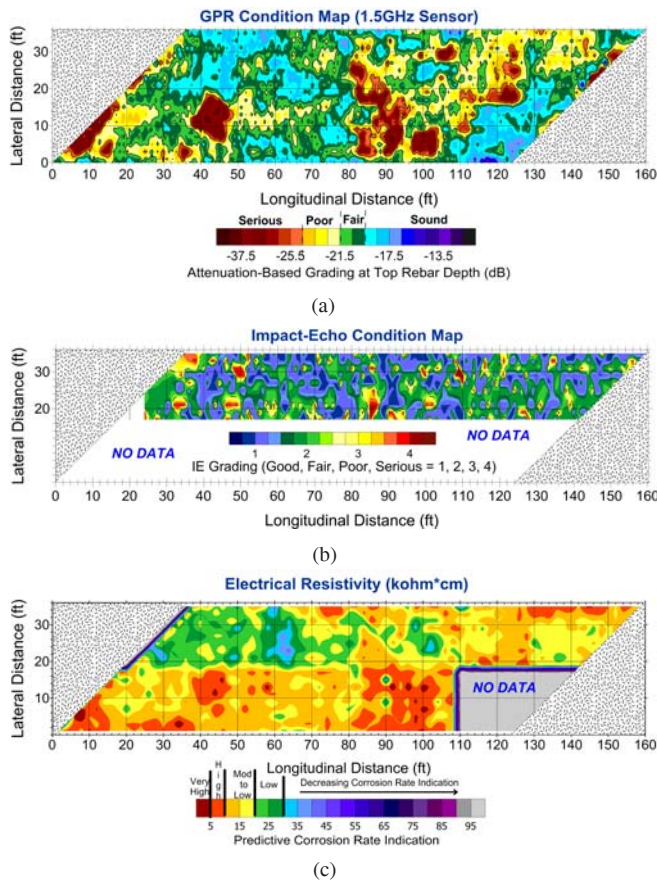


Fig. 9. The NDE inspection results on the Pohatcong Creek Bridge. (a) GPR mapping results. (b) Impact echo sensor mapping. (c) Electrical resistivity mapping.

V. CONCLUSIONS

The development and demonstration of an autonomous robotic system were presented for high-efficiency bridge deck inspection and evaluation. The autonomous inspection system was built on an omni-directional mobile robot and integrated with multiple NDE technologies such as GPR,

impact echo, and electrical resistivity. In this paper, we presented the mechatronic design to integrate the NDE sensors with the robot and the development of the robotic navigation system for high-performance bridge deck inspection. The high-accuracy robot localization scheme was built on the EKF-based fusion of the RTK GPS, IMU, and wheel odometry measurements. The robot motion control was designed through a concept of virtual robot following. The system performance was validated through experimental testing and field deployment. Extensive robotic NDE experiments and field deployments are among the ongoing research tasks.

REFERENCES

- [1] ASCE, "2009 Report Card for Americas Infrastructure," American Society of Civil Engineers, Tech. Rep., 2009, <http://www.infrastucturereportcard.org>.
- [2] N. Gucunski, F. Romero, S. Kruschwitz, R. Feldmann, A. Abu-Hawash, and M. Dunn, "Multiple complementary nondestructive evaluation technologies for condition assessment of concrete bridge decks," *Transp. Res. Rec.*, vol. 2201, pp. 34–44, 2010.
- [3] D. Huston, J. Cui, D. Burns, and D. Hurley, "Concrete bridge deck condition assessment with automated multisensor techniques," *Struct. Infrastruct. Eng.*, vol. 7, no. 7-8, pp. 613–623, 2011.
- [4] D. Hong and S. A. Velinsky and K. Yamazaki, "Tethered mobile robot for automating highway maintenance operation," *Robot. Comput.-Integ. Manuf.*, vol. 13, no. 4, pp. 297–307, 1997.
- [5] S. J. Lorenc and B. E. Handlon and L. E. Bernold, "Development of a robotic bridge maintenance system," *Automat. Constr.*, vol. 9, pp. 251–258, 2000.
- [6] P. C. Tung, Y. R. Hwang, and M. C. Wu, "The development of a mobile manipulator imaging system for bridge crack inspection," *Automat. Constr.*, vol. 11, pp. 717–729, 2002.
- [7] M. Trkov, F. Liu, J. Yi, and H. Baruh, "Study of concrete drilling for automated non-destructive evaluation and rehabilitation system for bridge decks," in *Proc. 2011 SPIE Conf. Nondestr. Charact. for Comp. Mat. Civil, Aero. Eng., Civil Infrastruct. Homeland Security V*, San Diego, CA, 2011, pp. 798 307–1–798 307–9.
- [8] F. Liu, M. Trkov, J. Yi, and N. Gucunski, "Modeling and design of percussive drilling for autonomous robotic bridge decks rehabilitation," in *Proc. IEEE Conf. Automat. Sci. Eng.*, Madison, WI, 2013.
- [9] J. K. Oh, G. Jang, S. Oh, J. H. Lee, B. J. Yi, Y. S. Moon, J. S. Lee, and Y. Choi, "Bridge inspection robot system with machine vision," *Automat. Constr.*, vol. 18, pp. 929–941, 2009.
- [10] R. S. Lim, H. M. La, Z. Shan, and W. Sheng, "Developing a crack inspection robot for bridge maintenance," in *Proc. IEEE Int. Conf. Robot. Autom.*, Shanghai, China, 2011, pp. 6288–6293.
- [11] F. Aghili and A. Salerno, "Driftless 3-D attitude determination and positioning of mobile robots by integration of IMU with two RTK GPSs," *IEEE/ASME Trans. Mechatronics*, vol. 18, no. 1, pp. 21–31, 2013.
- [12] K. Ohno, T. Tsubouchi, B. Shigematsu, and S. Yuta, "Differential GPS and odometry-based outdoor navigation of a mobile robot," *Adv. Robotics*, vol. 18, no. 6, pp. 611–635, 2004.
- [13] J. Yi, H. Wang, J. Zhang, D. Song, S. Jayasuriya, and J. Liu, "Kinematic modeling and analysis of skid-steered mobile robots with applications to low-cost inertial measurement unit-based motion estimation," *IEEE Trans. Robotics*, vol. 25, no. 5, pp. 1087–1097, 2009.
- [14] Z. W. Wang, M. Zhou, G. G. Slabaugh, J. Zhai, and T. Fang, "Automatic detection of bridge deck condition from ground penetrating radar images," *IEEE Trans. Automat. Sci. Eng.*, vol. 8, no. 3, pp. 633–640, 2011.
- [15] C. P. Connette, C. Parlitz, M. Hägele, and A. Verl, "Singularity avoidance for over-actuated, pseudo-omnidirectional wheeled mobile robots," in *Proc. IEEE Int. Conf. Robot. Autom.*, Kobe, Japan, 2009, pp. 4124–4130.
- [16] S. LaValle, *Planning Algorithms*. New York, NY: Cambridge University Press, 2006, also available at <http://planning.cs.uiuc.edu/>.
- [17] S. S. Ge and Y. J. Cui, "New potential functions for mobile robot path planing," *IEEE Trans. Robot. Automat.*, vol. 16, no. 5, pp. 615–620, 2000.